ELECTROMAGNETIC ANALYSIS OF THE INTERIOR PERMANENT MAGNET MOTOR FOR THE HYBRID ELECTRIC VEHICLE

Qurban Ali Shah Syed[*1] and Muharam Ali Shah[2]

[*1] Department of Electrical Engineering, The University of Larkano, Larkana, Pakistan
[2] Department of Electronics and Power Engineering, PNEC-NUST, Karachi, Pakistan
[*1] qurban.syed@uolrk.edu.pk, [2] muharam.shah786@gmail.com

ABSTRACT: This research paper deals with the electromagnetic analysis of the interior permanent magnet (IPM) motor for the hybrid electric vehicle (HEV). Like Toyota prius III traction motor, a V-typed single-layered IPM motor is investigated. A two-dimensional (2D) finite element analysis (FEA) methodology is discussed and adopted to compute the electromagnetic characteristics of the IPM motor, at no load and rated load with constant speed conditions. At no load, the cogging torque and back EMF of the IPM motor are computed, whereas at rated load and constant speed, the electromagnetic torque, magnet and iron core losses, and input electrical and output mechanical powers are computed using the 2D FEA. The cogging torque periodic cycle is determined using the analytical approach, and the current control angle is determined for the subsequent control strategies for the IMP motor. The electromagnetic output results are discussed in detail to understand their implications on the performance and efficiency of the IPM motor for the HEV traction application.

Index Terms:—Electromagnetic analysis, finite element analysis, hybrid electric vehicle, interior permanent magnet motor, permanent magnet motor

(Received 27.09.2025 Accepted 10.12.2025)

INTRODUCTION

The rapid expansion of the electric vehicle (EV) and hybrid electric vehicle (HEV) market has profoundly reshaped the landscape of electric machine technology [1]. The EV and HEV market is rapidly growing, propelled by the environmental regulations, thus it is driving significant advancements and specialized design requirements for the electric traction motors, with a strong focus on the permanent magnet (PM) technologies [2]. The operating range and drive-cycle requirements for the electric traction motors are different and challenging compared to conventional industrial electric motors [3]. Although induction motors and externally excited synchronous motors are also utilized by few manufacturers [1], [3], the PM motors are expected to maintain their dominant market share.

The PM motors, particularly the interior permanent magnet (IPM) motors and permanent magnet assisted synchronous reluctance motors (PMaSynRM), have become the preferred choice for the most vehicle manufacturers [1], [4]. The PMs are embedded in the IPM motor as well as in the PMaSynRM. However, unlike the IPM motor, the PMaSynRM relies heavily on the reluctance torque. Thus, the IPM motor has higher torque density because of PM and reluctance torque and also has very less cogging torque and torque ripples [5]. The common PM arrangements include single or double-layer V-shapes, spoke, flat or mixed variants for the IPM topologies [6]. The V-shape IPM motor shown in Fig. 1 has the flux focusing capability, therefore, it is considered due to its compact structure and high torque density.

The electromagnetic analysis of the IPM motor could be carried out by analytical, numerical or combination of different methods [7]. The FEA electrometric analysis is simple, reliable and conventionally used approach to investigate the IPM motor's electromagnetic characteristics [7]. A 3D FEA easily handles complex geometries and is accurate and reliable, however high computation time and system memory are required. The IPM motor is simple in structure and 2D FEA can easily be adopted to solve and investigate its electromagnetic characteristics.

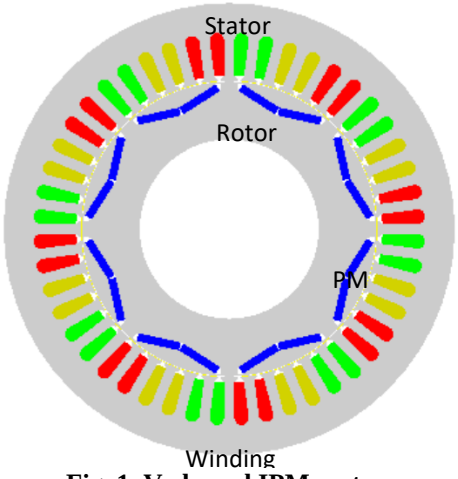

Fig. 1. V-shaped IPM motor.

This research paper is organized into 5 sections, where Section I provides brief introduction of the IPM motor, traction application and numerical analysis method. The details of the IPM motor structure, its geometrical design specifications are given in Section II. The 2D FEA methodology is discussed in Section III for the numerical analysis of the IPM motor. Section IV displays the no load and load characteristics of the IPM motor, and results are discussed in detail. Finally, the paper is concluded in Section V.

Table I: Specifications of the IPM motor.

Item	*Value*
Outer radius, mm	121
Airgap radius, mm	92.3
Shaft radius, mm	56
Axial length, mm	75
Stator slots	48
Pole pairs	4
Speed, rpm	1200

II. Interior Permanent Magnet Motor: The brushless IPM motor has a fixed stator that includes the yoke, slots, and windings, an air gap and a movable rotor with inserted PMs, as shown in Fig. 1. The stator of the IPM motor includes 48 slots for a 3-phase, Y-connection winding, whereas rotor of the IPM motor is slotted to place the 4 pole pairs V-shaped PMs. The inserted PMs are rare-earth NdFeB magnets with a remanence of 1.2 T, whereas iron of the stator as well as rotor of the IPM motor are of laminated M270-35A electrical steel.

The geometrical specifications of the IPM motor, designed for the HEV applications are given in Table I. The IPM motor's outer diameter is 242 mm, rotor's outer diameter is 184 mm, and an axial stack length of 75 mm, making it suitable for high-power density applications. The embedded magnets have a thickness of 5 mm. whereas the stator's slots opening width and depth are 2.0 and 1 mm, respectively. The airgap between the stator and rotor is 0.6 mm and it is without eccentricity for a smooth operation of the IPM motor for the HEV.

The rated performance characteristics of the IPM motor are for the high-performance HEV application, where both traction and generation functions are required. The IPM motor is designed to operate with a maximum bus voltage of 500 V, allowing it to handle a high-power demand efficiently. With a peak electromagnetic torque of 400 N.m, IPM motor delivers strong rotational force, essential for both propulsion and energy generation in HEV systems. The IPM motor reaches a maximum speed of 6000 rpm, enabling fast response and high-speed operation, while its peak power rating of 50 kW is achieved at 1200 ~ 1500 rpm, providing an excellent balance between electromagnetic torque and speed for the dynamic driving conditions of the HEV.

METHODOLOGY

The 2D FEA simulation method is adopted for the electromagnetic analysis at no-load and load characteristics at constant speed of the IPM motor. A 2D FEA involves several key steps, starting with the creation of the IPM motor geometry and mesh. Considering the repetitive components of the IPM motor, the base geometry of the IPM motor including a stator, rotor and airgap is created, however, airgap is divided into two parts, one stationery and other rotatory.

The rotor and stator of the IPM motor interact in a cyclic manner, and the periodic behavior is determined by the number of rotor poles and stator slots. The periodicity is defined, and boundary conditions are applied to reduce the computation time.

The meshing of the IPM motor geometry heavily influences the computation time, therefore, it is manually created. Thus, after the IPM motor's geometry, the mesh is created by specifying mesh density parameters, where a finer mesh is applied to regions with high magnetic flux or current concentration, such as the rotor, stator, and airgap, to capture detailed variations in magnetic and electric fields. The mesh density is typically adjusted between 0.5 and 1.0 to balance accuracy and computational efficiency, as shown in Fig. 2.

The transient magnetic 2D application is selected for computing the no load and load characteristics of the IPM motor. The physical properties, such as material characteristics, are defined and assigned to the specific regions of the IPM motor, such as, PMs and core. The next step in the physics procedure is to create mechanical and electrical sets, which define the speed of the rotor and supply current in winding scheme of the stator. These electrical and mechanical assigned components are essential for the IPM motor's movement and proper interaction with the stator's magnetic fields.

Once all the face regions of the 2D model of the IPM motor are defined and materials assigned, to proceed with the simulation. After completing the simulation, the results are analyzed to determine the IPM motor's performance.

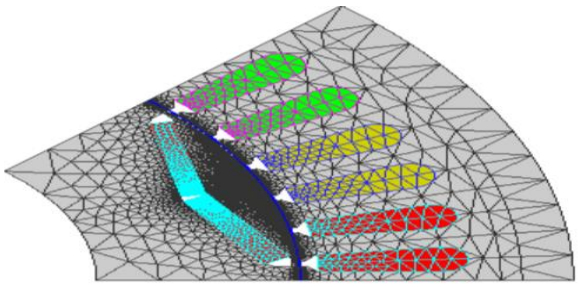

Fig. 2. Meshing of the IPM motor

RESULTS AND DISCUSSIONS

A 2D FEA is utilized to determine the cogging torque, back EMF, electromagnetic torque, electrical and mechanical power, and power losses using the Flux solver manual provided by the Altair ®, to investigate the performance of the V-shaped IPM motor for the HEV application.

A. ***No load characteristics:*** The cogging torque period is determined by the least common multiple (LCM) of the rotor slots and stator slots, calculated as 360° divided by the LCM [8]. Thus, for the configuration of the IPM motor with 8 rotor poles and 48 stator slots, the LCM is 48, resulting in a cogging torque period of 360/48 = 7.5°. The peak-to-peak cogging torque of the V-shaped IPM motor is 15.7 N.m, as shown in Fig. 3. The cogging torque characteristics of the IPM motor reveals the rotor's stable and unstable positions. A 0° rotor position corresponds to a stable position, conversely, other rotor positions, specially half of the cogging torque period i.e., 3.75° is an unstable position, and the cogging torque of the IPM motor pulls the rotor back to the stable position.

The back electromotive force (EMF) of the IPM motor is computed at a speed of 1000 rpm and at no load operating condition, as shown in Fig. 4. This computation is critical for determining the current control angle of the IPM motor. Thus, the angles of the different phase currents are identified by observing the zero-crossing points of the induced back EMF waveform for each phase. For a phase A, the mechanical angle is 7.5° corresponding to an electrical angle of 30°, thus, for phase B and phase C correspond to an electrical angle of 150°, and 270°, respectively. These values are essential for understanding the current and voltage phase relationships and for subsequent control strategies of the IPM motor.

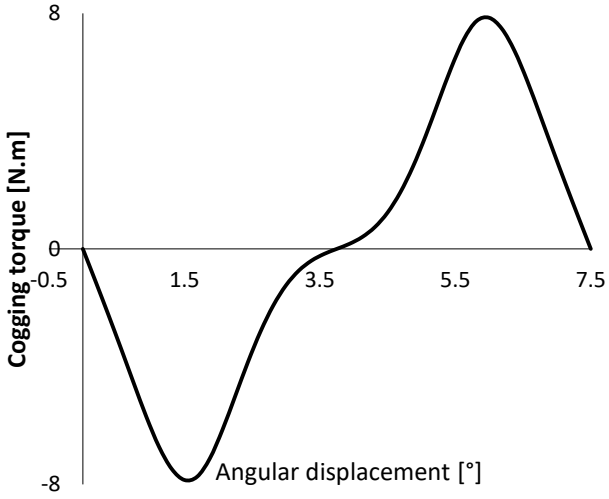

Fig. 3. Cogging torque of the IPM motor.

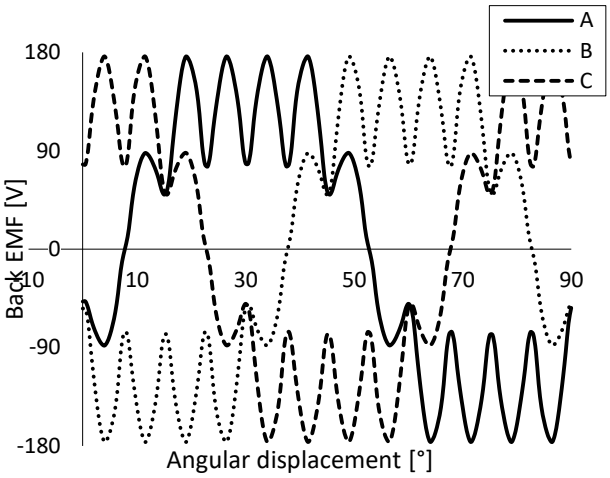

Fig. 4. Back EMF of the IPM motor.

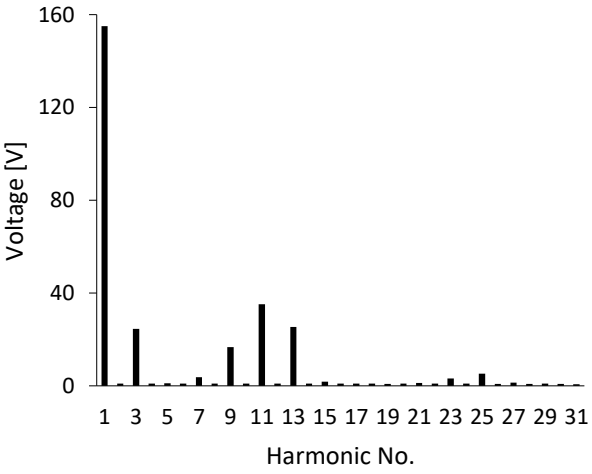

Fig. 5. Harmonic analysis of the Back EMF.

The Fast Fourier Transform (FFT) is applied on the full voltage cycle induced in phase A to analyze the harmonic content of the EMF. The FFT helps in understanding the frequency components present in the induced Back EMF, as shown in Fig. 5. Thus, harmonic analysis supports to identify and mitigate unwanted harmonics that lead to issues such as torque ripple, increased losses, and acoustic noise in the IPM motor.

B. ***Load characteristics at constant speed:*** The electromagnetic torque of the IPM motor is computed at rated load conditions, when a three-phase current is supplied. Thus, the magnetic field is distributed and potentially saturated within the motor components to develop the electromagnetic torque by the interaction of electrical current of the stator and magnetic field of the PMs, as shown in Fig. 6(a). However, flux density distribution differs significantly from the no-load conditions which is only due to the PMs alone, as shown in Fig. 6(b).

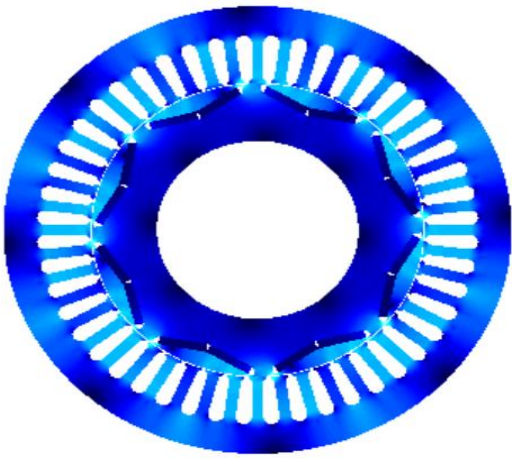

(a)

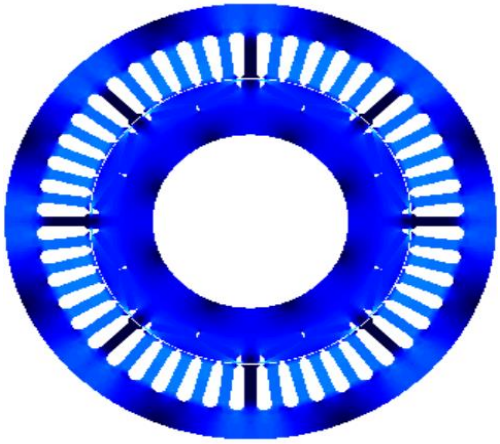

(b)

Fig. 6. Flux density distribution, where dark and light blue represents value of 0 T, and 3.34 T respectively.

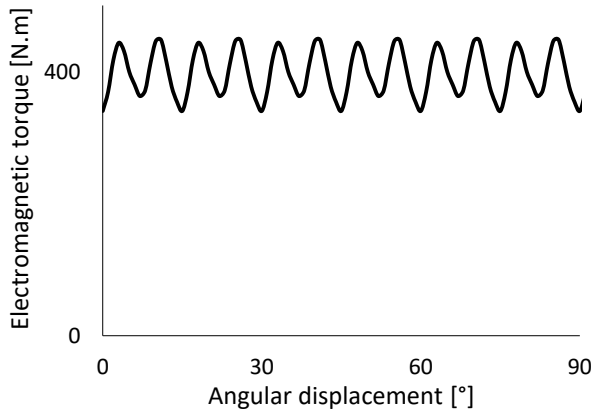

Fig. 7. Electromagnetic torque of the IPM motor.

The IPM motor has an average electromagnetic torque of 389.294 N.m under constant speed operation, as shown in Fig. 7. The electromagnetic torque curve shows torque ripples, which are attributed to the harmonic effects of the back EMF, and these ripples are crucial for the IPM motor design and control, as ripples lead to vibrations and noise. The initial rotor position for this case is set to 7.5° to align the phase current with the phase back EMF when the control angle is zero.

The eddy current loss in the magnets is computed at constant speed. The eddy current loss curve in Fig. 8 reveals the average value over the period for a PM pole is 2.70 W, thus, the eddy current losses in the PMs of the entire IPM motor due to is calculated to be 21.6 W. Similarly, the lamination steel (LS) iron loss is computed for the stator and iron core having laminated M27035A electrical steel material, using the 2D FEA. The average LS iron loss for the modeled part of Fig. 2 is 14.69 W, as shown in Fig. 9, leading to a total core loss of 117.52 W for the entire IPM motor. The total magnet and core losses are calculated by multiplying the computed loss results with the IPM motor's periodicity.

The input electrical power and output mechanical power of the IPM motor are computed and shown in Fig. 10, and Fig. 11, respectively. The average input electrical power is the multiplication of the three-phase input current and induced back EMF and is determined as 56.25 kW. It is negative because of the input power over one electric cycle. However, the output mechanical power is computed from the computed electromagnetic torque using the 2D FEA and rotational speed. The resulting output mechanical power is 48.92 kW. Thus, the efficiency of the IPM motor is determined to be 86.72%.

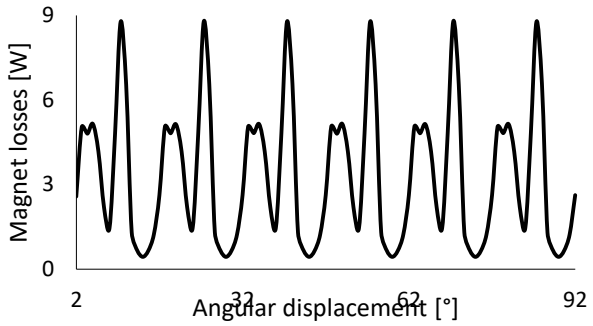

Fig. 8. Eddy current losses of the single PM pole.

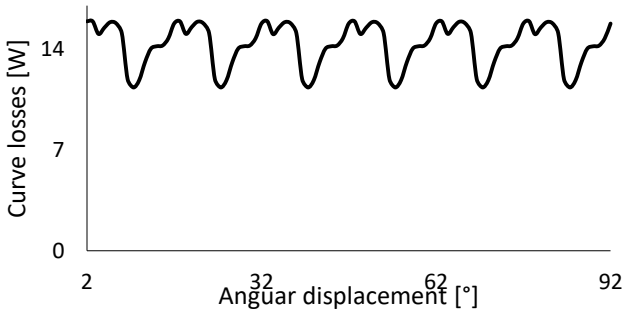

Fig. 9. Iron core losses of the IPM motor, having a single PM pole.

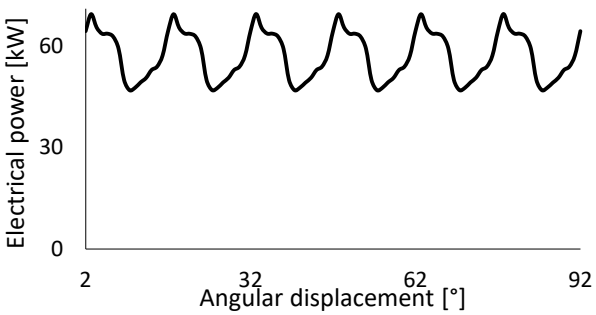

Fig. 10. Input electrical power of the IPM motor.

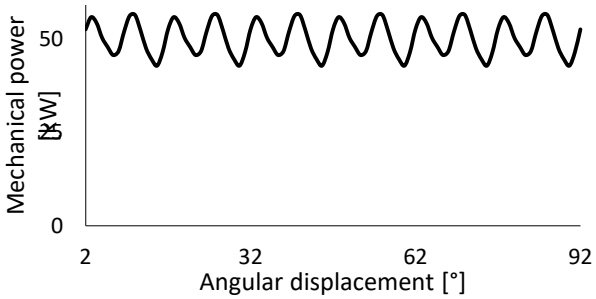

Fig. 11. Output mechanical power of the IPM motor.

Conclusion: The 2D FEA electromagnetic analysis is carried out at no load and at rated load of the brushless IPM motor, designed for the HEV traction and generation application. The cogging torque, a crucial parameter for motor smoothness and control at low speeds is computed, without stator current, speed of 1/6 rpm, and the rotor's angular position was varied over one slot pitch of 7.5°. The back EMF of the IPM motor under no-load electrical conditions is computed, using the 2D FEA, crucial in determining the current control angle necessary for effective IPM motor operation. Both cases provided fundamental insights into the IPM motor's inherent magnetic characteristics before stator current is supplied. The IPM motor is supplied by a 3-phase sine current at a constant speed to compute the motor performances, including electromagnetic or shaft torque, torque ripples, magnet eddy current losses and iron core losses, and overall efficiency.

This electromagnetic analysis provides a comprehensive foundation for understanding and optimizing the IPM motor's behavior in an HEV application. The sequential approach starting from intrinsic magnetic properties at no-load to detailed performance under load, provides a thorough characterization of the IPM motor. These results are essential for validating the IPM motor design choices, predicting its operational characteristics, and determining the control strategies for the IPM motor's integration into HEV traction application.

Acknowledgment: Corresponding author* acknowledges the support of Altair® for the 3D FEA license during the PhD research at the chair of Electrical Drives and Machines, FAU University of Erlangen-Nuremberg. The simulation and technical process is adopted from the Flux 2D solver manual.

REFERENCES

[1] A. Krings and C. Monissen, "Review and trends in electric traction motors for battery electric and hybrid vehicles," *2020 International Conference on Electrical Machines (ICEM)*, Gothenburg, Sweden, 2020, pp. 1807-1813, doi: 10.1109/ICEM49940.2020.9270946.

[2] D. Rimpas, S. D. Kaminaris, D. D. Piromalis, G. Vokas, K. G. Arvanitis, and C.-S. Karavas, "Comparative Review of Motor Technologies for Electric Vehicles Powered by a Hybrid Energy Storage System Based on Multi-Criteria Analysis," *Energies*, vol. 16, no. 6, p. 2555, Mar. 2023, doi: 10.3390/en16062555.

[3] D. Drexler, A. Kampker, H. Born, M. Nankemann, S. Hartmann, and T. Kulawik, "Advances in electric motors: A review and benchmarking of product design and manufacturing technologies," *Elektrotech. Inftech.*, Jul. 2025, DOI: 10.1007/s00502-025-01331-3

[4] M. Megrini, A. Gaga, and Y. Mehdaoui, "Review of Electric Vehicle Traction Motors, Control Systems, and Various Implementation Cards," *J. Operation Autom. Power Eng.*, vol. 13, no. 3, pp. 238-247, Aug. 2025. doi: 10.22098/joape.2024.13967.2077.

[5] M. Gobbi, A. Sattar, R. Palazzetti, and G. Mastinu, "Traction motors for electric vehicles: Maximization of mechanical efficiency – A review," *Appl. Energy*, vol. 357, p. 122496, Dec. 2024. https://doi.org/10.1016/j.apenergy.2023.122496.

[6] Q. A. S. Syed, *Spoke Type Axial Flux Permanent Magnet Motor and its Flux Switching Variants*, Ph.D. dissertation, Friedrich-Alexander-Universität Erlangen-Nürnberg, Technische Fakultät, 2025. DOI: 10.25593/open-fau-2172.

[7] Altair Engineering, Inc. (2025). *Altair Flux 2D: Finite element software for low-frequency electromagnetic and thermal simulations*. Available: https://altair.com/flux

[8] Q. A. S. Syed and I. Hahn, "Analysis of flux focusing double stator and single rotor axial flux permanent magnet motor," *2016 IEEE International Conference on Power Electronics, Drives and Energy Systems (PEDES)*, Trivandrum, India, 2016, pp. 1-5, doi: 10.1109/PEDES.2016.791432